Electronic Supplementary Material (ESI) for Polymer Chemistry.

Synthesis of Aromatic-doped Polycaprolactone with Tunable Degradation Behavior

Yawei Sun[a], Qiuyan Wang[b], Shuying Zhang[b], Hao Li [b], Jinli Zhang[a],

Daqing Li[b] (*), Wei Li[a] (*)

[a] School of Chemical Engineering & Technology, Tianjin University; Collaborative Innovation Center of Chemical Science and Chemical Engineering (Tianjin), Tianjin 300350, P. R. China.

[b] Key Laboratory of Cardiovascular Remodeling and Function Research, Chinese Ministry of Education and Chinese Ministry of Health, Qilu Hospital, Shandong University, Jinan 250061, Shandong, P. R. China.

*Corresponding author. Tel: +86-22-27404495, Fax: +86-22-27403389.

E-mail: liwei@tju.edu.cn

Assessment the Clotting Time

The round polymeric samples (ϕ14 mm, n=3) were placed in a 24-well plates, and incubated in 250 μL PPP at 37 °C for 30 min. Subsequently, 50 μL of the incubated PPP was added into a test cup, followed by adding 50 μL APTT agent and then incubated at 37 °C for 3 min. Then, a 50 μL solution of 0.025 M $CaCl_2$ was added to measure the APTT. For the PT test, 100 μL incubated PPP was added into a test cup and then mixed with 100 μL Thromborel S agent at 37 °C for 3 min before measuring the value of PT. For the TT test, 100 μL incubated PPP was added into a test cup, followed by adding 50 μL test thrombin agent (incubated for 15 min before utilization) and incubated at 37 °C for 2 min before measuring the TT.

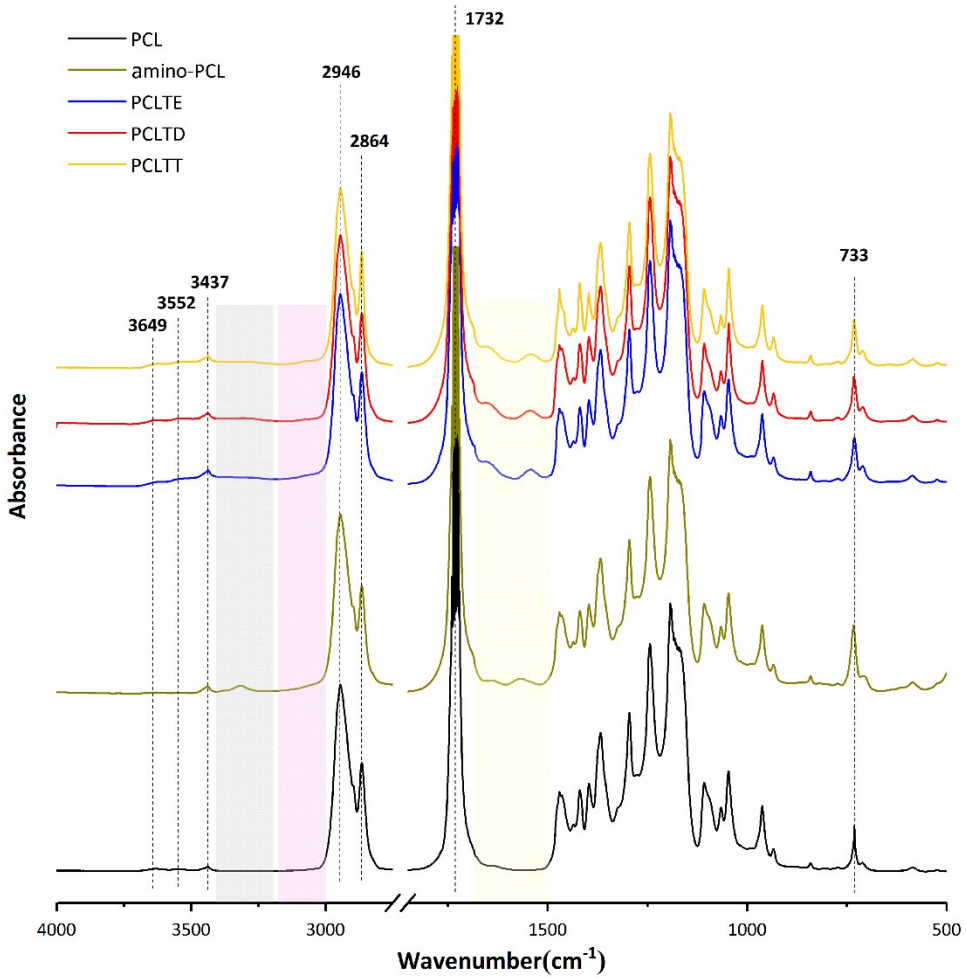

Fig. S1 FT-IR spectra of the pristine PCL, amino-PCL and three kinds of Aro-PCL including PCLTE, PCLTD and PCLTT.

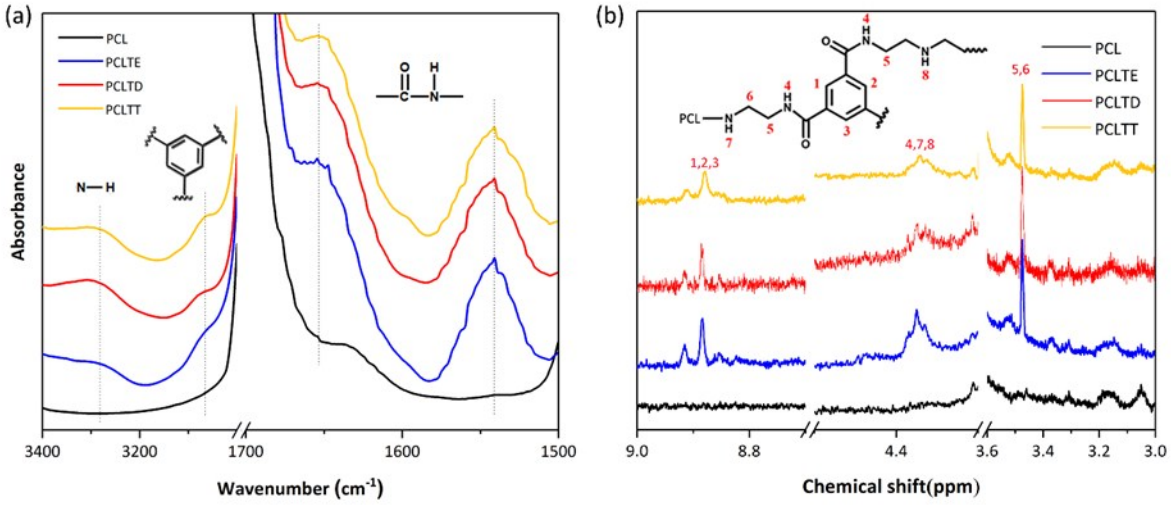

Fig. S2 FT-IR (a) and ^{1}H NMR (b) spectra of the pristine PCL and three kinds of Aro-PCL including PCLTE, PCLTD and PCLTT.

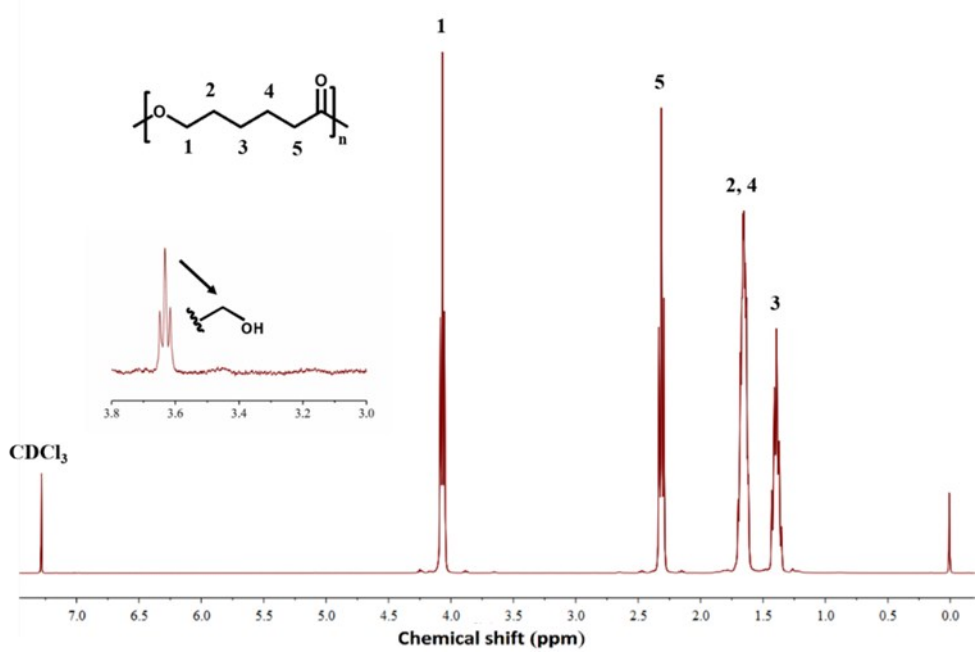

Fig. S3 ^{1}H NMR spectra of PCL.

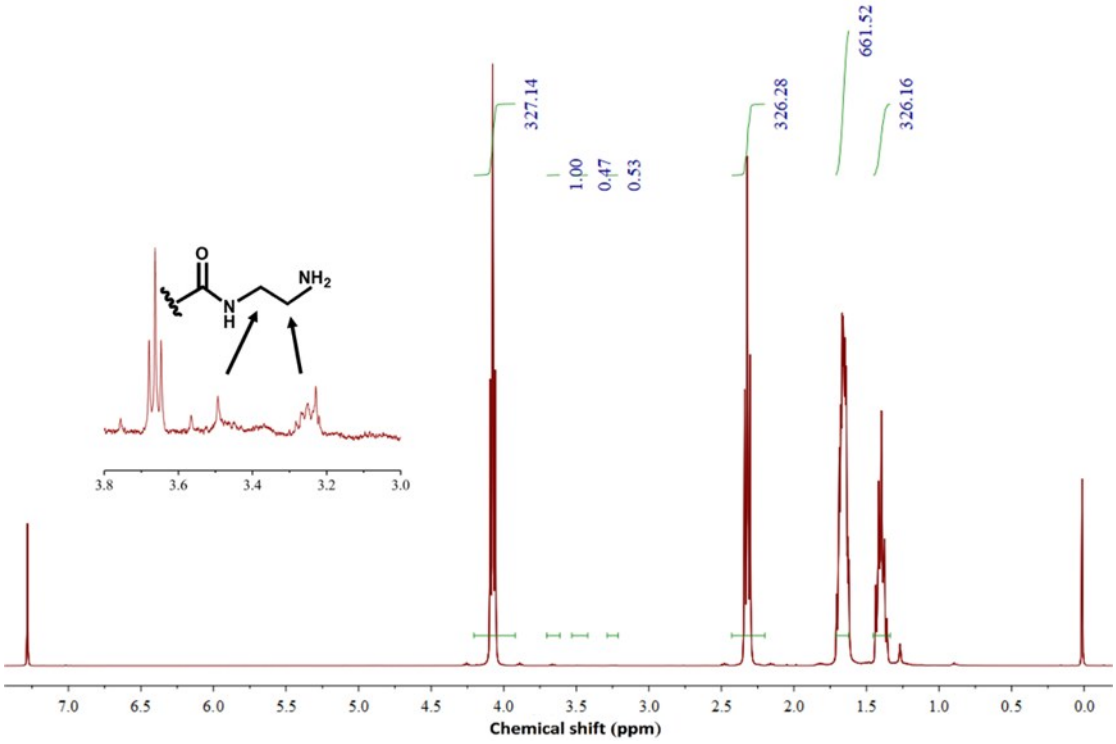

Fig. S4 ^{1}H NMR spectra of amino-PCL.

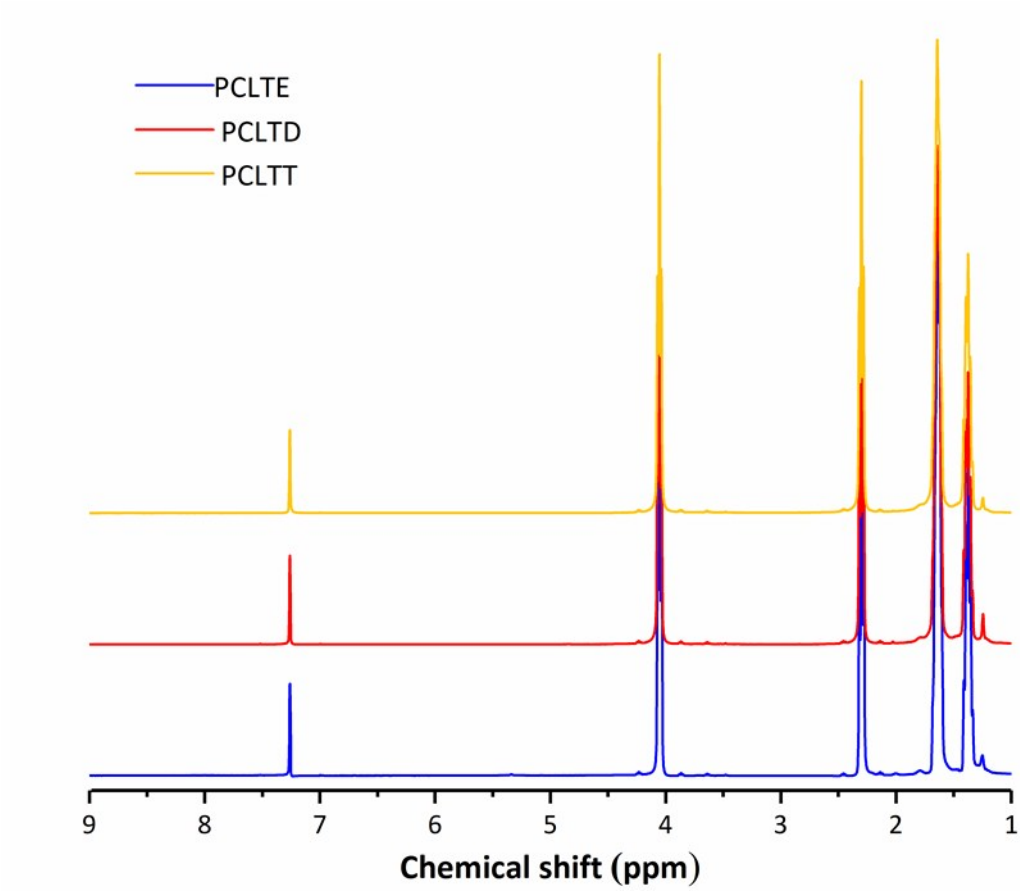

Fig. S5 ^{1}H NMR spectra of Aro-PCL.

Table S1 Characteristic parameters of synthesized polymer films

sample	M_n[a] ($\times 10^5$)	PDI[a]	T_g[b] (^oC)	T_m[b] (^oC)	X_c[b] (%)
PCL	1.06	1.85	-65.7	59.4	54.5
APCL	0.41	2.48	-	-	-
PCLT	0.47	2.91	-	-	-
PCLTE	0.974	1.89	-64.8	59.9	59.2
PCLTD	1.03	1.83	-65.4	59.7	51.2
PCLTT	1.08	1.82	-64.9	58.8	55.3

a Determined by GPC

b Determined by DSC, the X_c was calculated by the ratio of $\triangle H_m$, versus that of 100% crystalline PCL 139.5 J/g, $\triangle H_m$ was calculated via the integral area of the melt peak

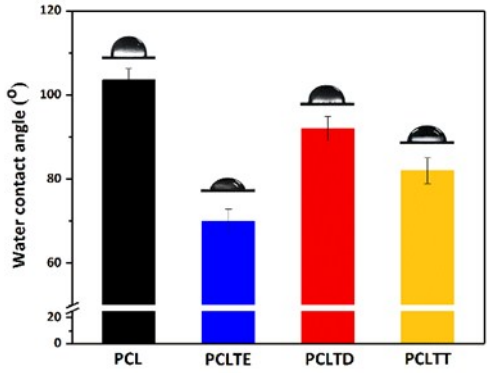

Fig. S6 Static water contact angles of the pristine PCL and Aro-PCL.

The hydrophilicity of the polymer films was evaluated by measuring the static water contact angles. As shown in Fig. S6, the water contact angle is 103.5 ± 2.8 ° for the pristine PCL, while it is respectively 70.0 ± 2.8 ° for PCLTE, 92.0 ± 2.8 ° for PCLTD, and 82.0 ± 3.0 ° for PCLTT. The decrease of the contact angle for the Aro-PCL is due to the hydrophilic amine groups introduced in the polymer films.

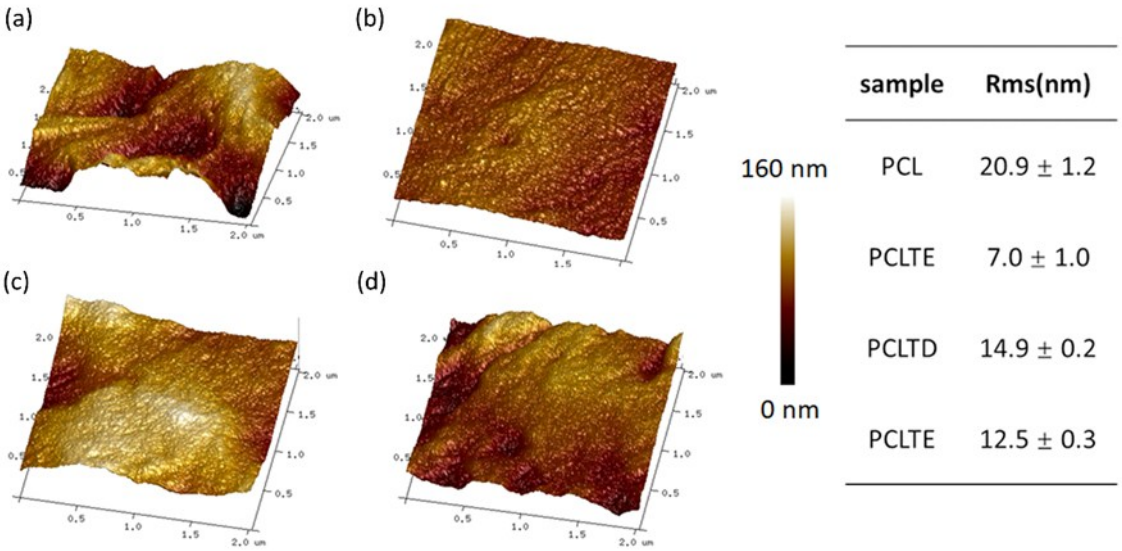

sample	Rms(nm)
PCL	20.9 ± 1.2
PCLTE	7.0 ± 1.0
PCLTD	14.9 ± 0.2
PCLTE	12.5 ± 0.3

Fig. S7 AFM images of the pristine PCL (a) and Aro-PCL including PCLTE (b), PCLTD (c) and PCLTT (d) films.

AFM images indicate that the surface roughness (Rms) of the Aro-PCLs is relative lower than that of the pristine PCL, which is in accord with the smaller spherulites formed in Aro-PCL, as displayed by POM (Fig. 3d). In addition, the phase image of AFM, observed in the tapping mode, can reflect the information about the surface

stiffness and the variation of Young's modulus, i.e., the bright color zone indicates the hard segments whereas the dark-colored represents the soft segments.[1] PCLTD exhibits the largest bright color zones, indicating that the mobility of soft segments in PCLTD is limited significantly owing to the linkage by the DETA.

The thermal properties were measured by DSC in the scanning range of 50-110 °C with the heating rate of 0.5 °C/min. The melt point of the pristine PCL is 59.8 °C, whereas it is 60.6 °C for PCLTD and a new inflection point appears at ca. 90 °C (shown in the inserted picture). It is attributed to the glass transition of incorporated moiety, suggesting the probability to form microphase separation in PCLTD.[2,3] Previously, Kato et al.[4] reported that the polymer chain close to the blocked junction point was more favorable for nucleation in the case of microphase separation.

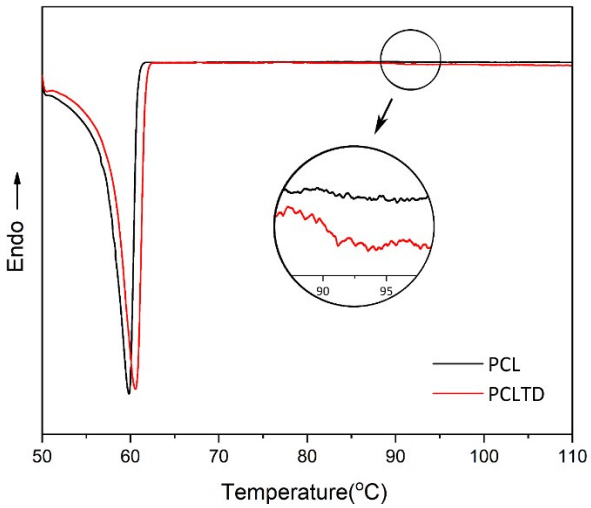

Fig. S8 DSC curves of the pristine PCL and PCLTD.

The prepared films were heated in oven at 110 °C for 5 min at first to erase the solvent history followed by cooling at room temperature for crystallization. Comparing with the relative absorbance curves of the Aro-PCLs and the pristine PCL films during solvent evaporation, the induction time is shorter in Aro-PCL films, probably owing to the lower solubility of Aro-PCLs in DCM. Considering the similar crystalline characteristic parameters of Aro-PCL and pristine PCL reflected by XRD patterns, the increased assemble rates are more attributed to the extra nucleation effect of the incorporated moieties in the polymers.

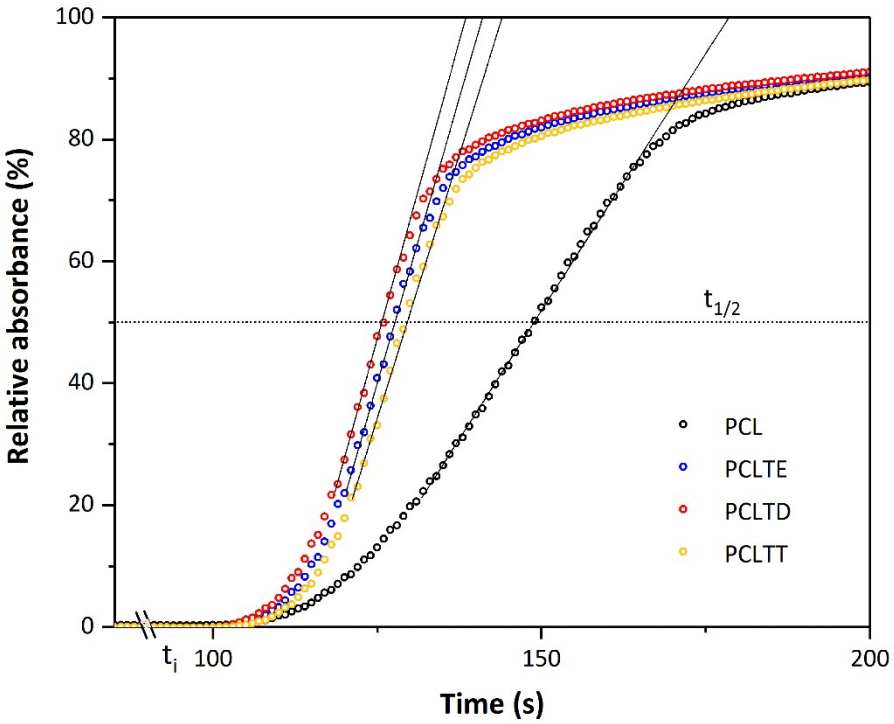

Fig. S9 Relative absorbance curves of the Aro-PCLs and the pristine PCL films.

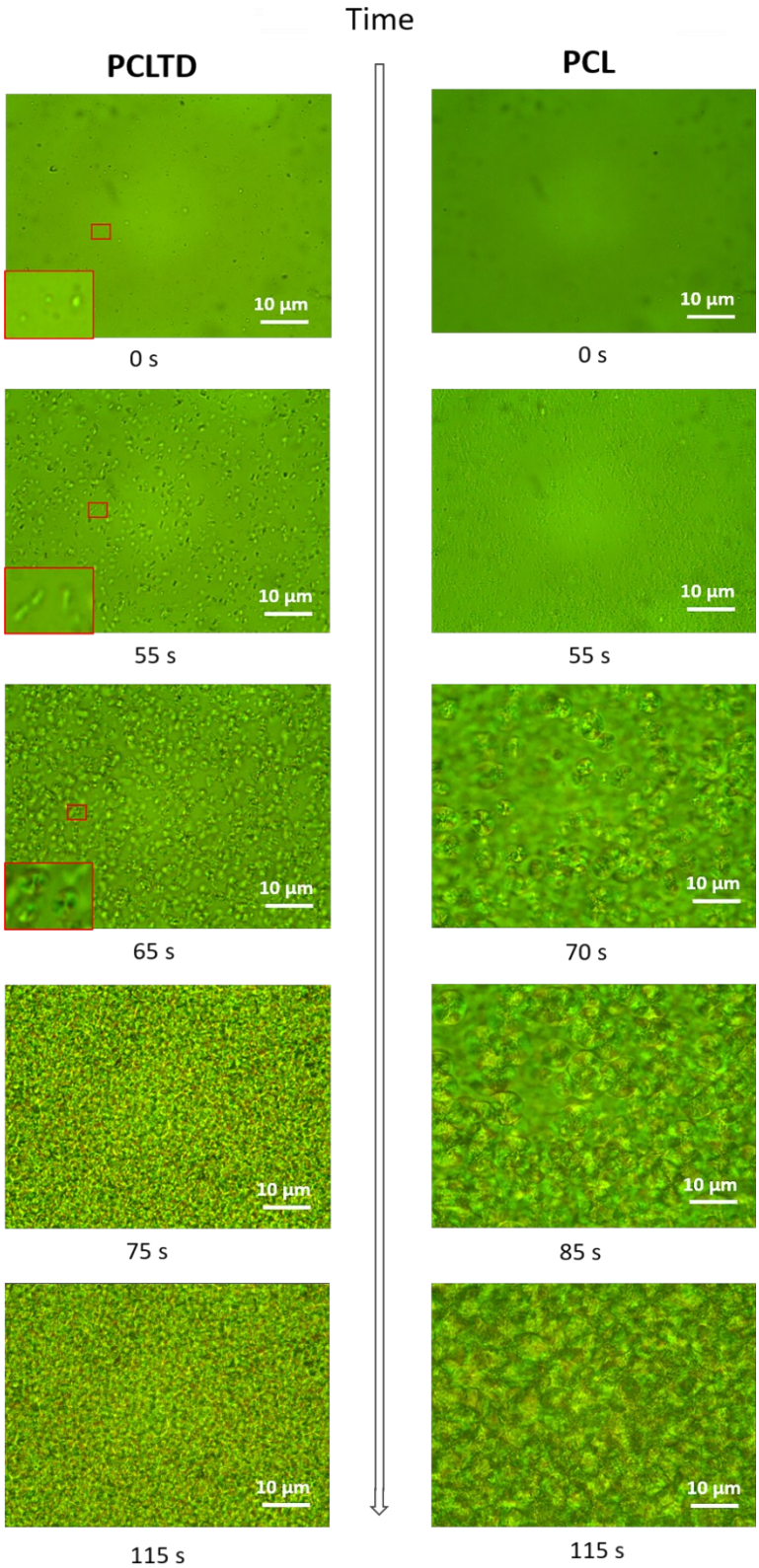

Fig. S10 Polarized optical micrographs of pristine PCL and PCLTD during nonisothermal crystallization.

Table S2. Crystalline characteristic parameters calculated by WAXD patterns

Sample	X_c[a] (%)	2θ (°)	hkl	d-space(Å)	I_{200}/I_{110}
PCL	57.8	21.480	110	4.133	0.20
		22.052	111	4.028	
		23.800	200	3.736	
PCLTE	61.2	21.539	110	4.122	0.33
		22.137	111	4.012	
		23.824	200	3.732	
PCLTD	54.6	21.580	110	4.115	0.40
		22.079	111	4.023	
		23.920	200	3.717	
PCLTT	58.6	21.540	110	4.1221	0.38
		22.085	111	4.0215	
		23.860	200	3.7262	

a Determined by XRD

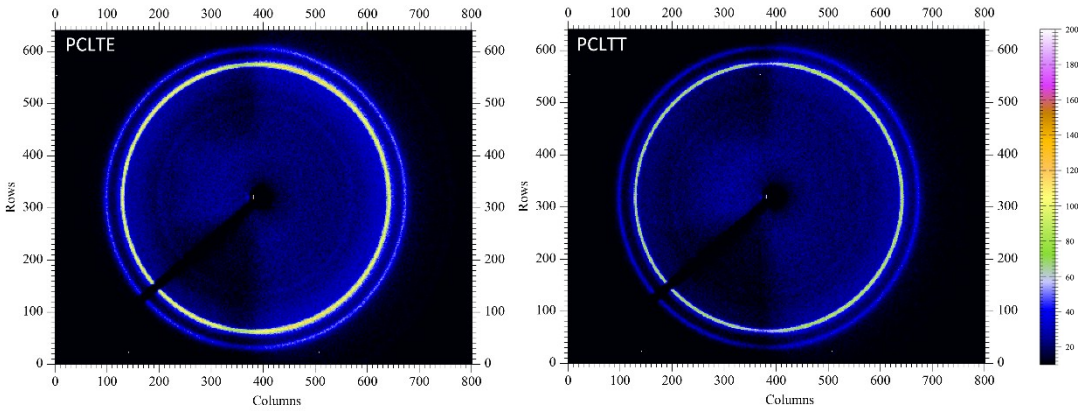

Fig. S11 2D-WAXD patterns of PCLTE and PCLTT.

The electron density (η) can be estimated by equation (R1) using method of group contribution.[5]

$$\eta_i = \frac{\rho_i n}{M_{w_i}} \quad \text{(R1)}$$

where ρ_i is mass density of introduced moiety, n is the number of electron and Mw_i is molecular weight. Take PCLTD as an example:

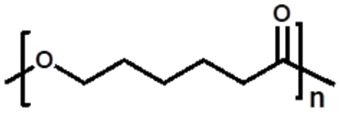

Number	Group	Mw	Mv	ρ	N

		(g/mol)	(cm^3/mol)	(g/cm^3)	(e)
5	$-CH_2-$	14	16.5	0.85	8
1	-C(=O)-	28	10.7	2.62	14
1	-O-	16	5.1	3.13	8
Sum		114	98.3	1.16	62

η_{PCL}=1.16×62/114=0.6307 mol e/cm3=379.68 e/nm^3

which is consistent with the data reported in literature that 393 e/nm^3 for crystalline PCL and 354 e/nm^3 for amorphous PCL at 25 °C, respectively.[6]

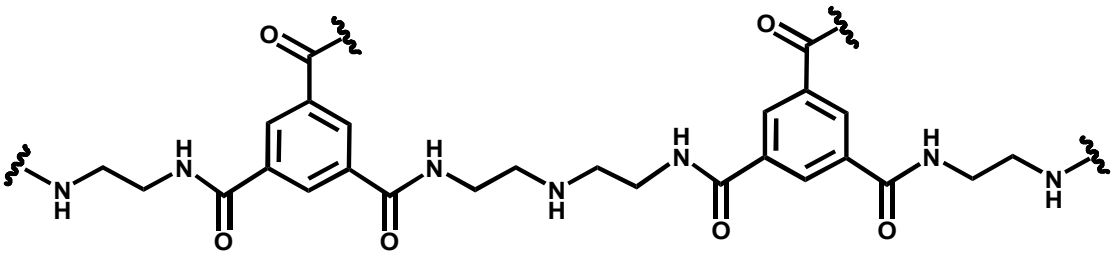

Number	Group	M_w (g/mol)	M_V (cm^3/mol)	ρ (g/cm^3)	N (e)
8	$-CH_2-$	14	16.5	0.85	8
6	-C(=O)-	28	10.7	2.62	14
7	-NH-	15	8.5	1.76	8
2	$-C_6H_3-$	75	33.4	2.25	39
Sum		535	322.5	1.66	282

η_{PCLTD}=1.66×282/535=0.875 mol e/cm^3=526.75 e/nm^3

Similarly, for PTLTE and PCLTT, the calculated electron density of PCLTE and PCLTT is 552.76 and 506.07 e/nm^3, respectively. All of them are much higher than the value of PCL. It is suggested that the incorporated moieties are excluded from the crystalline PCL segments and dedicate to the amorphous domain, thus leading the subdued intensities of SAXS peak, which governed by the electron density contrast between crystalline and amorphous domain.

Table S3. Mechanical properties of polymer films

sample	Yield strength (MPa)	Ultimate elongation (%)	Elastic modulus (MPa)	Tensile strength (MPa)	Radial strength (N)
PCL	15.2±0.4	686±40	242±2	22.7±1.5	1.75 ± 0.15
APCL	12.2±0.3	486±78	216±9	-	
PCLT	17.0±0.3	15±2	380±18	-	
PCLTE	16.6±0.04	823±42	440±12	37.4±3.3	2.85 ± 0.15
PCLTD	17.1±0.165	792±35	418±45	36.9±4.2	2.09 ± 0.53
PCLTT	16.7±0.175	857±32	364±22	38.2±2.0	1.96 ± 0.35

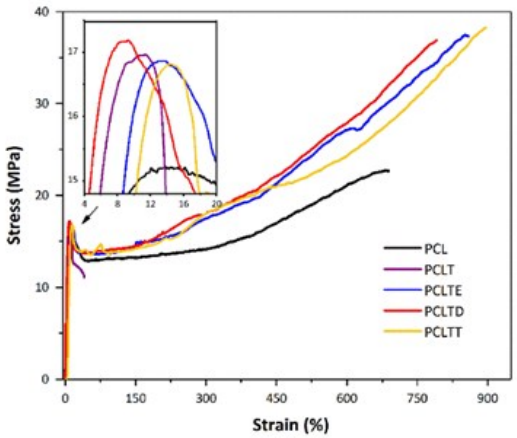

Fig. S12 Stress-strain curves for the pristine PCL, and Aro-PCL films.

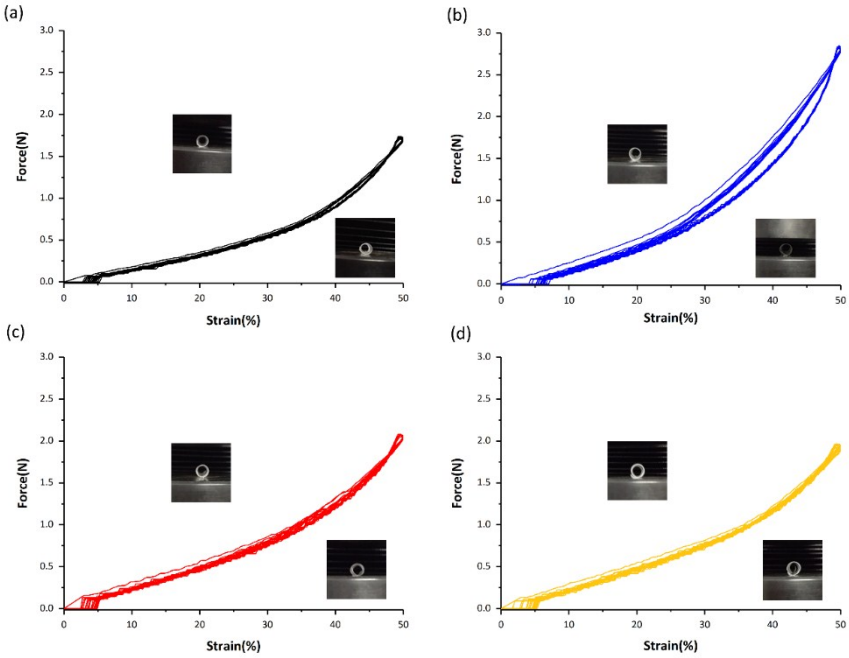

Fig. S13 The strain recovery and cyclic compress tests of PCL(a), PCLTE (b), PCLTD (c) and PCLTT (d) loops at 50% deformation.

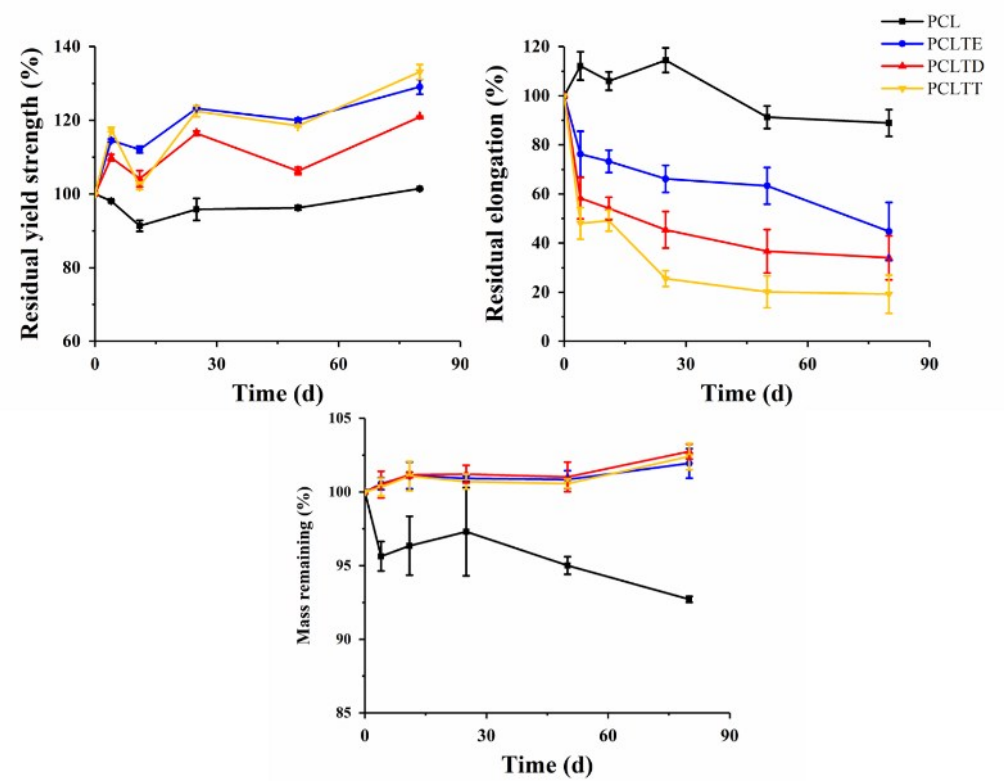

Fig. S14 Polymer film degradation: normalized yield strength(A), ultimate elongation (B), mass remaining (C) in Fe/H_2O_2 solutions.

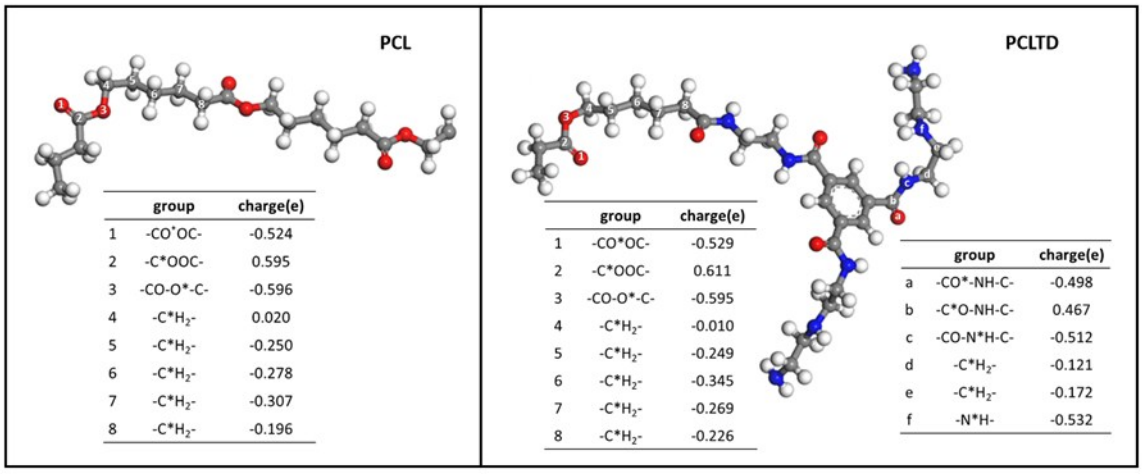

	group	charge(e)
1	-CO*OC-	-0.524
2	-C*OOC-	0.595
3	-CO-O*-C-	-0.596
4	-C*H_2-	0.020
5	-C*H_2-	-0.250
6	-C*H_2-	-0.278
7	-C*H_2-	-0.307
8	-C*H_2-	-0.196

	group	charge(e)
1	-CO*OC-	-0.529
2	-C*OOC-	0.611
3	-CO-O*-C-	-0.595
4	-C*H_2-	-0.010
5	-C*H_2-	-0.249
6	-C*H_2-	-0.345
7	-C*H_2-	-0.269
8	-C*H_2-	-0.226

	group	charge(e)
a	-CO*-NH-C-	-0.498
b	-C*O-NH-C-	0.467
c	-CO-N*H-C-	-0.512
d	-C*H_2-	-0.121
e	-C*H_2-	-0.172
f	-N*H-	-0.532

Fig. S15 Partial molecular structure model of the pristine PCL and the PCLTD, with the charge distribution.

Simulation of geometry optimization and charge distribution Geometry Optimization and Dynamics were tasked in the Forcite module (Material Studio, Accelrys Software, Inc.).[7] The calculation used a COMPASS forcefield and charge equilibration method (Q_{eq}). Initial configuration optimization was proceed through molecular dynamics (MD) simulations used a Canonical Ensemble (NVT). [8] In order to avoid this situation, it is necessary to optimize the molecular dynamics of the system at a higher temperature. At first, balanced at 298 K, then heating to 360 K to leaving the energy potential well of the initial state, passing over the energy barrier, and gradually cooling to 310 K and 298 K with time step of 500 ps, ensure optimization to a stable, relatively low energy state. At last, the geometry is optimized until the energy values no longer change and the charge in an equilibrium state.

It is reported that the electron-withdrawing oxygen atoms in water molecules attack the positively charged carbon atoms through a 2nd order nucleophilic substitution reaction during the hydrolytic process, resulting in the breaking of original chains.[9] We performed the molecular structure model to study the effect of doped aromatic ring and amine groups on the charge distribution in the polymer chain. As displayed in Fig. S15, the carbon atom in the ester groups of the pristine PCL shows the positive charge of 0.595 e. While in the PCLTD, the positive charged atoms include the carbon atom in the ester groups (0.611 e) and the carbon atom in the amide groups (0.467 e). It is reasonable to conclude that the doped aromatic

rings and the amide groups can change the electron density distribution greatly in the polymer chains, as proved by SAXS patterns in Fig. 3(c), which in turn modulates the variation of the molecule weight and the mechanical performance during hydrolytic degradation property of polycaprolactone.

References

1. C. Wang, Y. Zheng, Y. Sun, J. Fan, Q. Qin and Z. Zhao, *Polymer Chemistry*, 2016, **7**, 6120.
2. J. Hu, P. Yuan, K. Zeng and G. Yang, *Thermochimica Acta*, 2014, **590**, 30.
3. S. Nojima, Y. Ohguma, K. Kadena, T. Ishizone, Y. Iwasaki and K. Yamaguchi, *Macromolecules*, 2010, **43**, 3916.
4. R. Kato, S. Nakagawa, H. Marubayashi and S. Nojima, *Macromolecules*, 2016, **49**, 5955.
5. Y. He, *South China University of Technology*,2013. (in Chinese)
6. V. Crescenzi, G. Manzini, G. Calzolari and C. Borr, *Eurpean Polymer Journal*, 1972, **8**, 449
7. Y. Gao, W. Xu, D. Zhu, L. Chen, Y. Fu, Q. He, H. Cao and J. Cheng, *J Mater Chem A*, 2015, **3**, 4820.
8. Z. Rao, X. You, Y. Huo and X. Liu, *RSC Adv.*, 2014, **4**, 39552.
9. S. Lyu, J. Schley, B. Loy, D. Lind, C. Hobot, R. Sparer and D. Untereker, *Biomacromolecules*, 2007, **8**, 2301.